Acta Cryst. (1981). A**37**, 85–91

Novel Aspects of the Real Paracrystal

BY R. HOSEMANN, W. VOGEL AND D. WEICK

Fritz-Haber-Institut, Teilinstitut für Strukturforschung, Berlin-Dahlem, Federal Republic of Germany

AND F. J. BALTÁ-CALLEJA

Instituto de Estructura de la Materia, Serrano 119, *Madrid* 6, *Spain*

(*Received* 13 *December* 1979; *accepted* 25 *July* 1980)

Abstract

A revision of the mathematical concept of paracrystals is proposed. Hermann's [*Z. Electrochem.* (1940), **46**, 425–436] early theory of mesophases represents a special case of a paracrystal where the statistical parameters introduced were merely crystalline or gas-like. The theory of paracrystals removes the black-white picture of crystalline and amorphous phases by introducing 18 new statistical parameters into conventional crystallography. It is shown that a real paracrystal can be defined by a three-dimensional convolution polynomial in combination with an empirically derived α^* law. Hence, a missing corner-stone of colloid science is established.

I. Introduction

The theory of paracrystals was published for the first time by Hosemann (1949, 1950). Convolution operations, initially introduced by Ewald (1940) to define bounded crystals, were applied to describe quantitatively autocorrelation functions. These functions are known for liquids as pair-correlation functions or as Debye's *a priori* distance statistics (Debye, 1927) and are always spherically symmetric. In the case of ideal crystals autocorrelation functions are known as Patterson functions (Patterson, 1935). All these functions are convolution squares $Q(\mathbf{x})$ of a density distribution $\rho(\mathbf{x})$:

$$Q(\mathbf{x}) = \overset{2}{\tilde{\rho}}(\mathbf{x}) = \rho(\mathbf{x}) \widetilde{\rho(-\mathbf{x})} = \int \rho(\mathbf{y})\, \rho(\mathbf{y} + \mathbf{x})\, \mathrm{d}y^3. \quad (1)$$

This different nomenclature for the same operation is a typical feature of the schizoidal character of actual structure theories. M. von Laue (1960) pointed out in the preface of his famous book *Röntgenstrahl-Interferenzen* that a new branch of science is in progress which closes the gap between crystallography and theories of the liquid state.* On page 65 one finds another relevant statement.†

During the last 27 years the statements of von Laue have been, indeed, confirmed step-wise through a systematic experimental and theoretical research in the laboratories founded by him in 1952 at the Kaiser-Wilhelm-Institut für Physikalische Chemie in Berlin-Dahlem where he was Director. In the present paper we wish to show that there really exists a continuous transition from the short-range order of liquids up to the long-range order characteristic of conventional crystals. The gap is covered by the paracrystals. A large number of papers have been accumulating evidence in favour of them. Here we wish to recapitulate the essential points of this research work. Finally, we will comment on certain criticisms of the theory. According to von Laue a new branch of science is opening up.

II. The ideal paracrystal

The use of one-dimensional convolution polynomials has been known since the work of Landau (1937) and Ornstein & Zernike (1914). In the present study, however, we are concerned with a three-dimensional problem. Three vectors $\mathbf{a}_k$ ($k = 1, 2, 3$) span the unit cell of a paracrystalline lattice. In the special case of a primitive orthogonal lattice the three so-called coordination statistics $H_k(\mathbf{x})$ define the frequencies for

* 'Seit dem Erscheinen der 2. Auflage (1949) ist die Forschung über die Struktur der Kristalle und auch anderer Körper stürmisch fortgeschritten; es ist sogar, man könnte fast sagen, eine neue Wissenschaft entstanden über die Kristallbaufehler und ihre Folgen. Aber die Grundlagen der Theorie der Röntgeninterferenzen sind dadurch nicht berührt worden. Immerhin sind in § 10 R. Hosemann's Ergebnisse über den Bau der Parakristalle wenigstens in einfachster Form hinzugekommen.'

† 'Aber nicht nur bei Flüssigkeiten spielt die Nahordnung die für die Interferenzen entscheidende Rolle, es gibt vielmehr einen stetigen Übergang von ihr bis hin zur kristallinen Fernordnung. Solche Zwischenkörper bezeichnet man als 'Parakristalle'.'

0567-7394/81/010085-07$01.00

values $\mathbf{a}_k = \mathbf{x}$ in the autocorrelation function. Their first three moments are defined by

$$\int H_k(\mathbf{x})\,dx^3 = 1; \quad \int \mathbf{x} H_k(\mathbf{x})\,dx^3 = \bar{\mathbf{a}}_k;$$

$$(1/\bar{a}_i^2)\int (\mathbf{x} - \bar{\mathbf{a}}_k, \bar{\mathbf{a}}_i)^2 H_k(\mathbf{x})\,dx^3 = \Delta_{ki}^2;$$

$$g_{ki} = \Delta_{ki}/a_i. \tag{2}$$

Nine new variances g_{ki}^2 define here the fluctuation tensors g_{ki} of the statistics $H_k(\mathbf{x})$ and can have special orientations defined by nine Euler angles. In the theory of ideal paracrystals it is proposed, for convenience, that the vectors $\mathbf{a}_i$ and $\mathbf{a}_k$, touching each other within a given unit cell, do fluctuate without having any statistical correlation.

The probability for pairs such as $\mathbf{a}_i$ and $\mathbf{a}_k$ is given by $H_i(\mathbf{x})\,H_k(\mathbf{x})$. If one wishes to find the probability distribution for the vectors $\mathbf{a}_l + \mathbf{a}_k = \mathbf{y}$ one has to integrate over all vectors $\mathbf{a}_l$ with fixed values $\mathbf{y}$, finding as a result:

$$H(\mathbf{y}) = \int H_i(\mathbf{x})\,H_k(\mathbf{y} - \mathbf{x})\,dx^3 = \widehat{H_i H_k}. \tag{3}$$

$H_i(\mathbf{x})$ represents the probability for the position of the atom (1,0) and $H_k(\mathbf{y})$ for the atom (0,1) (Fig. 6). If we further use both vectors $\mathbf{x}$ and $\mathbf{y}$ to define the position of the lattice point (1, 1) then evidently there will be no correlations between $\mathbf{x}$ and $\mathbf{y}$. The opposite sides of this lattice cell are, nevertheless, identical. The whole ideal paracrystal consists therefore of a network of parallelepipeds (see Fig. 1). The convolution polynomial

$$z(\mathbf{x}) = \sum_{pqr} H_{pqr}(\mathbf{x})$$

with

$$H_{pqr}(\mathbf{x}) = P(\overbrace{x-0)\,H_i\,H_i \ldots}^{p\text{ times}}\overbrace{H_i\,H_k\,H_k \ldots}^{q\text{ times}}\overbrace{H_k\,H_l\,H_l \ldots H_l}^{r\text{ times}} \tag{4}$$

represents the autocorrelation function of an unbounded paracrystal. The Fourier transform (symbol $\mathcal{F}$) of $z(\mathbf{x})$ is the paracrystalline lattice factor $Z(\mathbf{b})$. This factor can be easily calculated using the convolution theorem of the $\mathcal{F}$ transform which states that

$$\mathcal{F}\,\widehat{H_l H_k} = F_l F_k \text{ if } F_i(\mathbf{b}) = \mathcal{F}(H_i);$$

$$F_k(\mathbf{b}) = \mathcal{F}(H_k) \tag{5}$$

where the vector $\mathbf{b}$ expands in reciprocal space. Thus,

$$Z(\mathbf{b}) = \mathcal{F}(z) = \prod_{k=1}^{3} K_k; \quad K_k = \mathrm{Re}\,\frac{1 + F_k}{1 - F_k}. \tag{6}$$

Each K_k factor has the maxima $(1 + |F_k|)/(1 - |F_k|)$ if

$$(\mathbf{a}_k\,\mathbf{b}) = \mathbf{h}_k \quad (h_k \text{ integer}), \tag{7}$$

which are the well known 'Laue conditions'. Contrary to the case of crystals, minima with the value $(1 - |F_k|)/(1 + |F_k|)$ different from zero, also exist if

$$(\mathbf{a}_k\,\mathbf{b}) = h_k + \tfrac{1}{2}. \tag{8}$$

The integral width δb_k of the maxima parallel to the direction of $\mathbf{a}_k$ is given by

$$\delta b_k = (1/2\bar{a}_k)(1 - |F_k|) \simeq (1/\bar{a}_k)(\pi g_{kk} h_k)^2 \tag{9}$$

(see Appendix I). In the case of crystals δb_k is zero because F_k is a Fourier transform of the point function $H_k(\mathbf{x})$ and hence $|F_k| = 1$. According to Ewald (1940) a bounded paracrystal can be obtained if one multiplies the density distribution function $\rho(\mathbf{x})$ by a shape function $s(\mathbf{x})$ which is equal to unity inside the lattice and zero outside it. Then $z(\mathbf{x})$ should be multiplied with the convolution square $\widehat{s^2}(\mathbf{x})$ of $s(\mathbf{x})$, which is, according to (1), defined by $\widehat{s(\mathbf{x})\,s}(-\mathbf{x})$. Its Fourier transform $S^2(\mathbf{b})$ is the shape factor of Ewald. For the intensity function $I(\mathbf{b})$ one finally obtains

$$I(\mathbf{b}) = (1/v)\,\widehat{Z\,|S^2|}\,.\,f_0^2 \tag{10}$$

where v is the volume $\bar{\mathbf{a}}_i\bar{\mathbf{a}}_k\bar{\mathbf{a}}_i$ of a lattice cell, and f_0^2 is the structure factor.

Fig. 2 offers an example of a paracrystalline two-dimensional structure. Here the small coins are packed two-dimensionally in an atttempt to build up a cubic primitive lattice. However, 10% of larger coins which are distributed over the lattice statistically disturb the cubic arrangement. This is the essential assumption for the occurrence of a paracrystalline lattice: point defects, which produce local microstrains overlapping with each other, are irregularly distributed

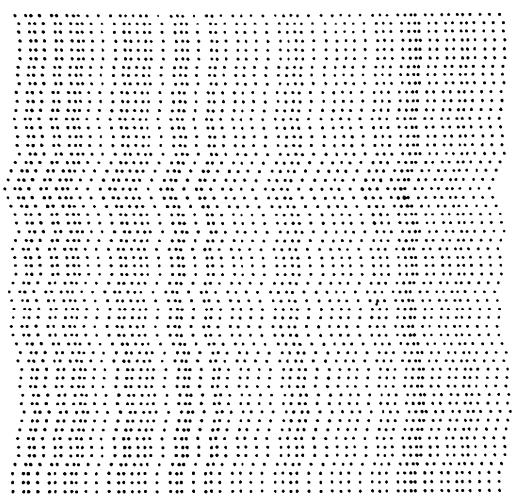

Fig. 1. A two-dimensional computer-simulated ideal paracrystal. The horizontal lines and the vertical netplanes are identical. The ideal paracrystal can grow unlimitedly.

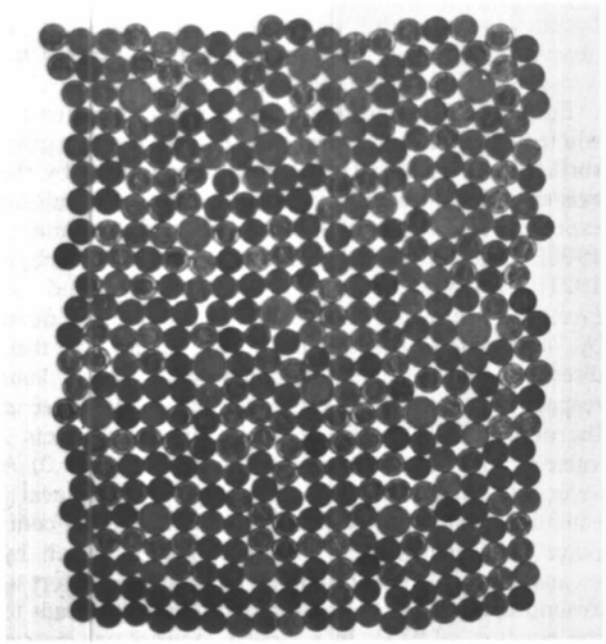

Fig. 2. Model of a real paracrystal built up by cubic packing of small coins disturbed by a small amount of larger ones. Each lattice cell has a different shape. The disorder of the lattice is larger at the boundaries than in the centres. This was first mentioned by Brämer (1975) and Brämer & Ruland (1976). The real paracrystal has, therefore, always a limiting size depending on the degree of distortion.

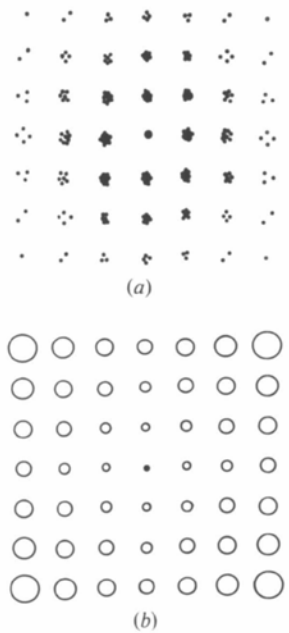

Fig. 3. The autocorrelation function (Q function defined by equation 1) of 4 × 4 point atoms arranged in a cubic paracrystalline two-dimensional lattice. (*a*) A single Q function; (*b*) half-widths of an assembly of individual Q functions leading to a continuous density distribution defined by the convolution polynomial of equation (3). According to a real paracrystal the half-widths of the maxima at the boundaries amount only to 20 to 30% of the nearest-neighbour distances.

over the lattice. If we assume that the nodes of a lattice are built by 4 × 4 coins and construct their convolution square defined by (1), we obtain 16 × 16 distance vectors, which lie with one end at the origin (0,0) (Fig. 3). The 16 points at $x = 0$ represent the distance vectors of each point with itself. The 12 points adjacent to the left or to the right side define the position of their nearest neighbours, the following eight points show the distances between the next-nearest neighbours, and so on. In practice, the observable convolution square is the sum of thousands of individual point statistics. The single points are no longer detectable on account of the always limited resolving power. Therefore, continuous density clouds defined by a bounded autocorrelation function appear (see equation 10):

$$(1/v)\, z(\mathbf{x}) \overset{2}{\tilde{s}}(\mathbf{x}). \tag{11}$$

The half widths of the single function $H_{pqr}(\mathbf{x})$ are plotted in Fig. 3(*b*). These widths increase according to the laws of statistics with the square root of the distance from the centre. The integral widths of the reflections are given by the width of the folding product of $Z(\mathbf{b})$ with $|S(\mathbf{b})|^2$ according to (10). The integral width δb_s of $|S|^2$ along a reciprocal cell edge is given by $(1/\mathbf{a}_k)(1/N_k)$, where N_k is the number of netplanes within the paracrystal. If, for instance, both functions Z and $|S|^2$ are Lorentzian-like, then the total width δb is given by

$$\delta b = \delta b_k + \delta b_s. \tag{12}$$

By substitution of (9) into (12) we obtain from the $\delta b - h^2$ plot the values of N_k and g_{kk}:

$$\begin{aligned}\delta b &= (1/a_k)\,[(1/N_k) + (\pi g_{kk}\, h)^2] \\ &= (1/a_k\, N_k)\,[1 + (\pi\alpha^*\, h)^2].\end{aligned} \tag{13}$$

III. The real paracrystal

The values of N_k and g_{kk} have been derived for different paracrystalline samples from the analysis of the δb–h^2 plot on a very large number of X-ray diffraction patterns. The evaluation of these data leads to the empirical relation

$$\sqrt{N_k}\, g_{kk} = \alpha^*, \quad 0{\cdot}1 \lesssim \alpha^* \lesssim 0{\cdot}2. \tag{14}$$

Fig. 4 illustrates the plot of the experimental values of $\sqrt{N_k}$ against $1/g_{kk}$ (Baltá-Calleja & Hosemann, 1980). All samples under investigation lie between the above mentioned boundaries of α^*. Doped metals like the ammonia catalyst have the smallest g values of ~1% (Hosemann, Preisinger & Vogel, 1966; Ludwiczek, Preisinger, Fischer, Hosemann, Schönfeld & Vogel, 1978). Polymer single crystals from solution have somewhat larger g values (Höhne & Wilke, 1970). Melt-crystallized polyethylene and two-dimensional model structures have g values of ~2% and more (Čačković, Loboda-Čačković & Hosemann, 1973).

Melts and pyrolytic graphite with $g \simeq 4\%$ and more have g values near the gaseous state $g > 30\%$ (Steffen, 1976; Steffen & Hosemann, 1976*a*,*b*).

The physical meaning of (14) is shown in Fig. 5. The right part of an autocorrelation function of a two-dimensional paracrystal shows that the fluctuation Δ_N of point distances between the first and $(N + 1)$th netplane increases proportionally with $\sqrt{N}$. If Δ_N reaches the limiting value $\alpha^* \bar{d}$ ($\bar{d}$ = mean netplane distance) then the curvature of this boundary netplane becomes so large that the valence angles between the atoms within this netplane cannot withstand the stresses any longer and break their bindings.

Equation (14) is of fundamental importance for the whole field of colloid science and tells us that large inner surfaces can be stabilized if they are produced by the existence of microparacrystals. A computer simulated experiment illustrates this point (Janke & Hosemann, 1978). The '*a priori* distance statistics' (Debye, 1927) of two vectors $\mathbf{a}_1$ (horizontal) and $\mathbf{a}_2$ (vertical) are given independently from each other by a Monte-Carlo method. The angles of their directions between the horizontal and vertical lines respectively may be of the order of α^*. We start at the origin (0,0) (see Fig. 6): The computer selects a value $\mathbf{a}_1$ and, hence, the position of the atom at (1,0). A value $\mathbf{a}_2$ in the vertical direction is subsequently generated, reaching the position (1,1). Now the computer supplies two new values $\mathbf{a}_1$ and $\mathbf{a}_2$ which by means of a circle construction – drawing the vectors $\mathbf{a}_2$ around the point (0,0) and $-\mathbf{a}_1$ around (1,1) – leads to the position of (0,1). In a similar manner one passes through $(\bar{1},1)$ over the $(\bar{1},\bar{1})$ and so on. The computer draws progressively, in this way, a spiral of lattice points around the origin until the distance fluctuations between lattice points become so large that the two circles cannot intersect with each other anymore. Fig. 7 shows the paracrystalline lattice drawn by the computer and the arrow indicates where the paracrystal construction is stopped. Fig. 8 illustrates the Fraunhofer diffraction pattern of the model and Fig. 9 shows the corresponding δb–h^2 plot which yields the values $N = 43 \pm 4$ and $g = 2{\cdot}1 \pm 0{\cdot}2\%$. These data agree within the errors of the experiment with the values $N = 45$ and $g = 2\%$ introduced into the model. This experiment demonstrates that (9) to (14), derived for the ideal paracrystal, are also applicable for real paracrystals having non-parallelepipedic-shaped lattice cells. More-

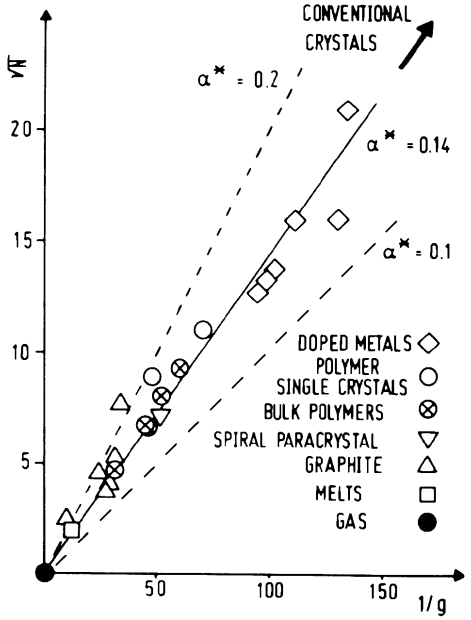

Fig. 4. The experimentally observed $\sqrt{N}$ values of natural microparacrystals as a function of the reciprocal paracrystalline g values (equation 2).

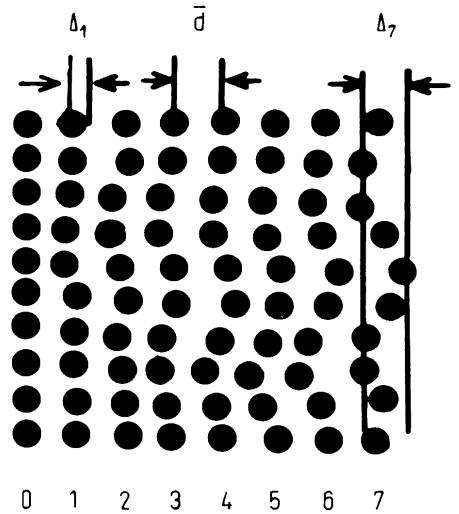

Fig. 5. The physical meaning of the α^* law (equation 14). For details see text.

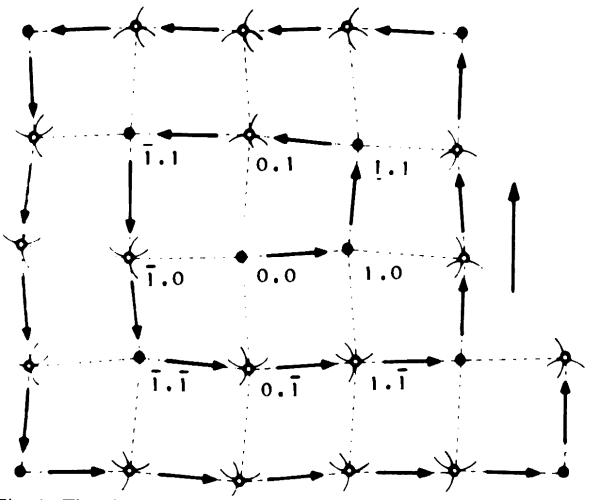

Fig. 6. The circle construction of the spiral paracrystal. See text for details.

over, the α^* value of the model is 0·14 in accordance with the values obtained for natural microparacrystals (see Fig. 4). The reason for the reliability of (10) for natural paracrystals stems from the fact that the value of α^* is small in comparison with unity. The consequence of this is that, similarly to the case of the spiral paracrystal, all vectors $\mathbf{a}_i$ along one line of lattice points of a real paracrystal can fluctuate in length and are practically independent from those of the adjacent lines. The existing correlations influence mostly their directions. This is of physical significance, because atomic bond angles are much more flexible than bond lengths. Even at the boundaries of the lattice the single vector lines $\sum_i \mathbf{a}_i$ have lengths which differ statistically by not more than $\alpha^* \bar{a}_i$. The directions of the $\mathbf{a}_i$ vectors of an ideal three-dimensional paracrystal are, therefore, influenced by correlations with adjacent $\mathbf{a}_i$ lines leading to a change of their direction by an angle φ smaller than α^*. Let us suppose for convenience that the statistics $H(\varphi)$ of these correlation-induced changes of direction are constant for $|\varphi| \leq \alpha^*$ and normalized to unity. Since

$$\int_0^{\alpha^*} 2\pi \sin\varphi \, \mathrm{d}\varphi \simeq 2\pi\alpha^{*2}/2,$$

one obtains

$$H(\varphi) = \begin{cases} 1/\pi\,\alpha^{*2} \text{ for } & |\varphi| \leq \alpha^* \\ 0 & |\varphi| > \alpha^* \end{cases}.$$

If the vector $\mathbf{a}_i$ under consideration deviates in an ideal paracrystal by an angle β_i from its mean direction, then $\delta = \overline{\cos(\beta_i + \varphi)} - \overline{\cos\beta_i}$ is the mean change of the length projection of each vector $\mathbf{a}_i$ in a spiral paracrystal. One obtains

$$\delta = -\tfrac{1}{4}\alpha^{*2}\,\overline{\cos\beta} - \tfrac{2}{3}\alpha^*\,\overline{\sin\beta} \qquad (15)$$

(see Appendix II). $\overline{\sin\beta}$ is much smaller than α^*, hence, δ is smaller than 0·01. The correction of the correlation lies, therefore, within the limits of error and can be neglected.

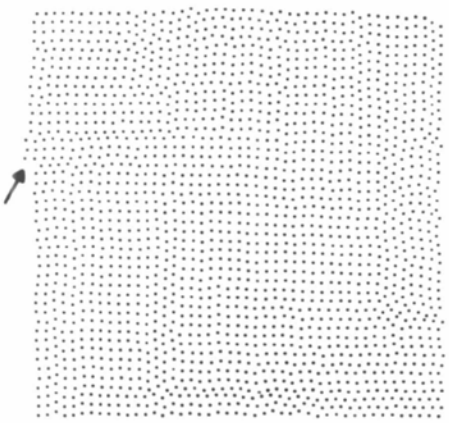

Fig. 7. A computer-simulated spiral paracrystal with $g_{11} = g_{22} = 0{\cdot}02$. The arrow indicates the break-down of the circle construction.

IV. Objections to the concept of paracrystal

Several objections which have appeared in the literature are caused by certain misunderstandings. Some authors have associated the paracrystalline domains in polymers with the transition zones between the crystalline and amorphous phases (Kakudo & Kasai, 1972). Other objections arise because the α^* law is neglected (Perret & Ruland, 1971; Brämer, 1975; Brämer & Ruland, 1976). These authors, for instance, do not take into account that in (10) the shape factor $|S|^2$ is strongly correlated with the lattice factor Z by the α^* law in (13).

The conclusion drawn by Perret & Ruland (1971) stating that 'it is impossible to bring the theory of paracrystals into agreement with the experimental results of small-angle scattering' is certainly questionable because they neglect the α^* law and use much too large values for $Ng^2 = 0{\cdot}2$ (instead of $\alpha^{*2} \simeq 0{\cdot}02$). With correct α^* values the ideal paracrystal certainly furnishes somewhat larger X-ray small-angle intensities than pure particle scattering. This is because in the ideal paracrystal three families of netplanes, where

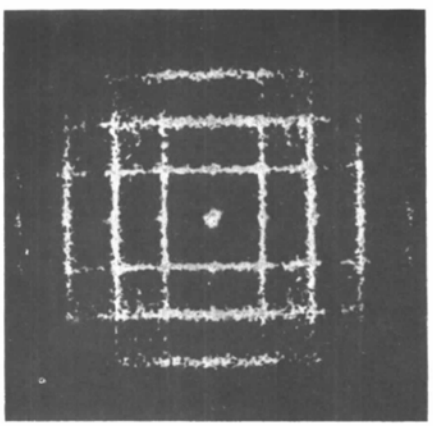

Fig. 8. Laser–Fraunhofer diffraction pattern of Fig. 7 similar to that of the ideal paracrystal.

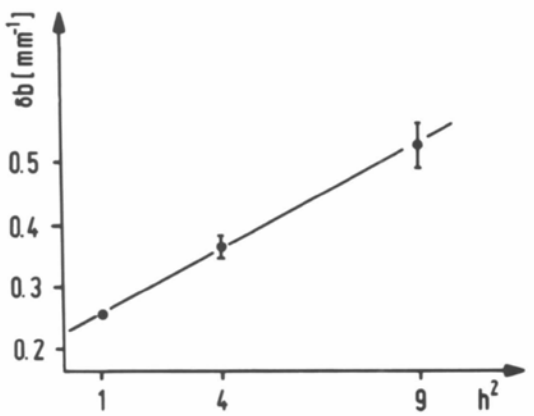

Fig. 9. δb–h^2 plot of the $(h,0)$ reflections of Fig. 8.

all netplanes fluctuate as rigid entities, occur (Fig. 1). This effect can be eliminated numerically in the analysis of small-angle scattering (Weick & Hosemann, 1980).

The considerations exposed in § III suggest that there is no reason whatsoever to take literally the model of the ideal paracrystal. Equations (9) to (12) can also be, in fact, applied to wide-angle scattering of the real paracrystal where such rigid entities no longer exist (See Fig. 9).

In another case Ruland (1979) argues that δb–h^2 plots can also be obtained from polycrystalline material, if it is under stress. Until now only a linear relationship between δb and h has been discussed in solid-state physics. Vogel (1967) for instance found it in cold-deformed pure α-Fe (see Fig. 10). Since shape factor and lattice function have Lorentzian-like profiles, the linear relation (12) can be used and one finds

$$\delta b = (1/aN)\,[1 + N(\Delta a/a)\,h]. \qquad (16)$$

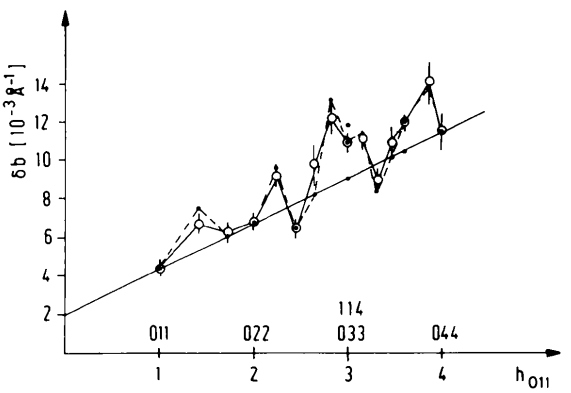

Fig. 10. Integral widths δb of the reflection of cold-deformed pure α-Fe.

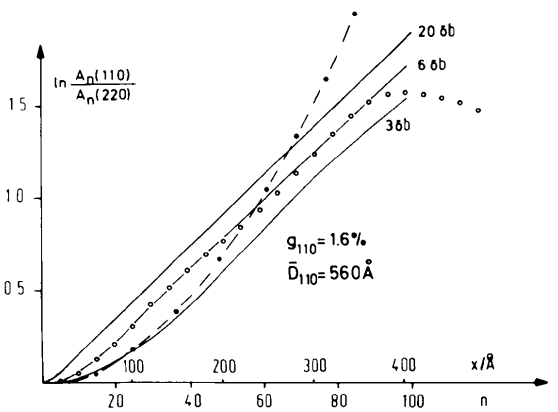

Fig. 11. Fourier analysis of reflection profiles 110 and 220 of melt-crystallized linear polyethylene. —— Paracrystalline distortion $g_{110} = 1{\cdot}6\%$. The number $n\delta b$ gives the domain $(n/2)\,\delta b \leq |b - h/a|$ within which the Fourier transform of the reflection h was carried out. --- Calculated from Gaussian-type profiles of microstrained crystals.

Δa is the standard deviation of the lattice constants a of single crystallites. $N\Delta a/a$ has, for instance, the value 1·2 in the example of Fig. 10.

How can δb–h^2 diagrams be produced by microstrains? We found two conditions which simultaneously must be realized:

(1) S^2 and the lattice function are 'Gaussian'-like;

(2) $N\Delta a/a \lesssim 0{\cdot}3$.

Instead of (16) one then obtains

$$\delta b = (1/aN)\{1 + [N(\Delta a/a)h]^2\}^{1/2}$$
$$\simeq (1/aN)\{1 + \tfrac{1}{2}[N(\Delta a/a)\,h]^2\}. \qquad (17)$$

The similarity with (13) is obvious. $\frac{1}{2}(N\Delta a/ah)^2$ is replaced by $(\pi\alpha^* h)^2 = y$. The approximation on the second line of (17) works within $\gamma \sim 6\%$ for $y \lesssim 0{\cdot}5$ (Appendix III). At least three orders of reflections must be observable, if crystallites with the quadratic approach of (17) can be identified. Therefore $N\Delta a/a$ must be smaller than 0·5 or $\alpha^* < 0{\cdot}1$. Glocker (1958) discussed that iron, contrary to Fig. 10, can have $N\Delta a/a$ values down to 0·28 if cold worked and quickly annealed above the recovery temperature. Interpreted as paracrystalline, such material would not belong to all the paracrystals investigated until now, because its α^* value and line profiles are of a different type.

For completeness it may be mentioned that Vogel, Haase & Hosemann (1974) have generalized the Fourier method of Warren & Averbach (1950). With the help of the Fourier transforms A_{110} and A_{220} of two reflections one can differentiate easily between microstresses and paracrystalline distortions. An example is given in Fig. 11.

In our next paper it will be shown that the analysis of melts and polymers carried out with the help of the paracrystal theory leads to novel results with regard to thermal fluctuations and isothermal compressibility.

APPENDIX I

The three-dimensional function $F_k(\mathbf{b})$ is given in the Guinier approximation by

$$F_k(\mathbf{b}) = |F_k(\mathbf{b})| \exp(-2\pi i \mathbf{b}\bar{\mathbf{a}}_k)$$

with

$$|F_k(\mathbf{b})| \simeq \exp(-2\pi^2 g_{kk}^2 h_k^2). \qquad (AI.1)$$

The $K_k(\mathbf{b})$ function of (6) consists of a background $(1 - |F_k|)/(1 + |F_k|)$. The maxima at the position of the Laue condition in (7) have, hence, a value

$$\frac{1 + |F_k|}{1 - |F_k|} - \frac{1 - |F_k|}{1 + |F_k|} = \frac{4|F_k|}{1 - |F_k|^2}. \qquad (AI.2)$$

The integral value of a reflection is given by

$$(1/\bar{a}_k)\left(1 - \frac{1 - |F_k|}{1 + |F_k|}\right) = (1/\bar{a}_k)\frac{2|F_k|}{1 + |F_k|}. \qquad (AI.3)$$

The quotient of (AI.3) and (AI.2) is defined as integral width

$$\delta b = (\tfrac{1}{2}\tilde{a}_k)(1 - |F_k|) \simeq (1/a_k)(\pi g_{kk} h_k)^2,$$

if one introduces the approximation in (A1.1).

APPENDIX II

The relative change of the mean length $\sum \mathbf{a}_i$ of the ideal paracrystal is given by the statistical correlation

$$\begin{aligned}\delta &= \cos\overline{(\beta_i + \varphi)} - \overline{\cos\beta_i} \\ &= \overline{\cos\beta}\,\overline{(\cos\varphi - 1)} - \overline{\sin\beta}\,\overline{\sin\varphi}. \qquad \text{(AII.1)}\end{aligned}$$

Since $|\varphi| \lesssim \alpha^*$ it follows from (14) that

$$\begin{aligned}\overline{\cos\varphi} &= (2/\alpha^{*2}) \int_0^{\alpha^*} (1 - \tfrac{1}{2}\varphi^2)\,\varphi\,\mathrm{d}\varphi = 1 - \tfrac{1}{4}\alpha^{*2} \\ \overline{\sin\varphi} &= (2/\alpha^{*2}) \int_0^{\alpha^*} (\varphi - \tfrac{1}{6}\varphi^3)\,\varphi\,\mathrm{d}\varphi \\ &= \tfrac{2}{3}\alpha^*(1 - \tfrac{1}{10}\alpha^{*2}) \qquad \text{(AII.2)}\end{aligned}$$

and (15) follows.

APPENDIX III

The paraboloid character of the root in (17) can be defined by γ and is a quantitative measure of reliability of its tentative δb–h^2 approximation (see Table 1).

Table 1. *The paraboloid character of the root of equation* (17)

$\gamma = |(1 + y)/(1 + 2y)^{1/2} - 1| \times 100.$
$y = (\pi\alpha^* h)^2$ or $= \tfrac{1}{2}(N\Delta a/ah)^2$.

y	0·03	0·05	0·2	0·5	1	3	10
$1 + y$	1·03	1·05	1·20	1·50	2·0	4	11
$(1 + 2y)^{1/2}$	1·03	1·05	1·18	1·41	1·73	2·7	4·6
γ (%)	0	0	1·4	6	15	51	140

References

BALTÁ-CALLEJA, F. J. & HOSEMANN, R. (1980). *Ber. Bunsenges. Phys. Chem.* **84**, 91–95.

BRÄMER, R. (1975). *Acta Cryst.* A**31**, 551–660.

BRÄMER, R. & RULAND, W. (1976). *Makromol. Chem.* **177**, 3601–3612.

ČAČKOVIĆ, H., LOBODA-ČAČKOVIĆ, J. & HOSEMANN, R. (1973). *J. Polym. Sci. Symp.* **42**, 591–604.

DEBYE, P. (1927). *Phys. Z.* **28**, 135–147.

EWALD, P. P. (1940). *Proc. Phys. Soc. London*, **52**, 167–172.

GLOCKER, R. (1958). *Materialprüfung mit Röntgenstrahlen*, p. 353. Berlin: Springer-Verlag.

HERMANN, C. (1940). *Z. Elektrochem.* **46**, 425–436.

HÖHNE, G. & WILKE, W. (1970). *Kolloid Z. Z. Polym.* **241**, 994–995.

HOSEMANN, R. (1949). *Z. Phys.* **127**, 16–39.

HOSEMANN, R. (1950). *Z. Phys.* **128**, 1–35, 465–492.

HOSEMANN, R., PREISINGER, A. & VOGEL, W. (1966). *Ber. Bunsenges. Phys. Chem.* **70**, 796–862.

JANKE, M. & HOSEMANN, R. (1978). *Prog. Colloid Polym. Sci.* **64**, 226–231.

KAKUDO, M. & KASAI, N. (1972). *X-ray Diffraction of Polymers*, p. 148. Amsterdam–London–New York: Kodanske Elsevier.

LANDAU, L. D. (1937). *Zh. Eskp. Theor. Fiz.* **7**, 1227–1235.

LAUE, M. VON (1960). *Röntgenstrahl-Interferenzen*, 3. Aufl. Frankfurt: Akademische Verlagsgesellschaft.

LUDWICZEK, H., PREISINGER, A., FISCHER, A., HOSEMANN, R., SCHÖNFELD, A. & VOGEL, W. (1978). *J. Catal.* **51**, 326–337.

ORNSTEIN, L. S. & ZERNIKE, F. (1914). *Proc. Acad. Sci. Amsterdam*, **17**, 793–806.

PATTERSON, A. L. (1935). *Z. Kristallogr.* **90**, 517–554.

PERRET, R. & RULAND, W. (1971). *Kolloid Z. Z. Polym.* **247**, 835–843.

RULAND, W. (1979). *Verh. Dtsch. Phys. Ges.* **7**, 1184.

STEFFEN, B. (1976). *Phys. Rev. B*, **13**, 3227–3231.

STEFFEN, B. & HOSEMANN, R. (1976*a*). *Phys. Rev. B*, **13**, 3232–3238.

STEFFEN, B. & HOSEMANN, R. (1976*b*). *Ber. Bunsenges. Phys. Chem.* **80**, 710–712.

VOGEL, W. (1967). *Gitterstörungen* 1. *und* 2. *Art in binären Legierungen und komplexen Metallverbindungen.* Diploma, Freie Univ. Berlin.

VOGEL, W., HAASE, J. & HOSEMANN, R. (1974). *Z. Naturforsch. Teil A*, **29**, 1152–1158.

WARREN, B. E. & AVERBACH, B. L. (1950). *J. Appl. Phys.* **21**, 595–603.

WEICK, D. & HOSEMANN, R. (1980). *Colloid Polym. Sci.* **258**, 450–550.